

# JTok: ON TOKEN EMBEDDING AS ANOTHER AXIS OF SCALING LAW VIA JOINT TOKEN SELF-MODULATION

Yebin Yang<sup>12</sup>, Huaijin Wu<sup>1</sup>, Fu Guo<sup>2</sup>, Lin Yao<sup>2</sup>, Xiaohan Qin<sup>1</sup>, Jingzhi Wang<sup>1</sup>,  
Debing Zhang<sup>2</sup>, Junchi Yan<sup>1\*</sup>

<sup>1</sup> School of AI, Shanghai Jiao Tong University

<sup>2</sup> Hi Lab, Xiaohongshu Inc.

## ABSTRACT

LLMs have traditionally scaled along dense dimensions, where performance is coupled with near-linear increases in computational cost. While MoE decouples capacity from compute, it introduces large memory overhead and hardware efficiency challenges. To overcome these, we propose token-indexed parameters as a novel, orthogonal scaling axis that decouple model capacity from FLOPs. Specifically, we introduce **Joint-Token (JTok)** and **Mixture of Joint-Token (JTok-M)**, which augment Transformer layers with modulation vectors retrieved from auxiliary embedding tables. These vectors modulate the backbone via lightweight, element-wise operations, incurring negligible FLOPs overhead. Extensive experiments on both dense and MoE backbones, spanning from 650M (190M + 460M embedding) to 61B (17B + 44B embedding) total parameters, demonstrate that our approach consistently reduces validation loss and significantly improves downstream task performance (e.g., +4.1 on MMLU, +8.3 on ARC, +8.9 on C-Eval). Rigorous isoFLOPs analysis further confirms that JTOK-M fundamentally shifts the quality–compute Pareto frontier, achieving comparable model quality with 35% less compute relative to vanilla MoE architectures, and we validate that token-indexed parameters exhibit a predictable power-law scaling behavior. Moreover, our efficient implementation ensures that the overhead introduced by JTOK and JTOK-M remains marginal.

## 1 INTRODUCTION

The development of large language models (LLMs) is closely linked to the scaling laws of Transformer architectures [50]. The conventional approach to enhancing model performance involves increasing the number of parameters and training tokens, which typically yields smooth power-law improvements [23; 15]. However, both FLOPs and GPU memory requirements scale approximately linearly with model size, while the availability of high-quality text data is becoming increasingly limited. As a result, simply scaling dense models leads to diminishing marginal returns and may even cause performance degradation in data-constrained settings [51; 24].

To address the inefficiencies of dense scaling, Mixture-of-Experts (MoE) architecture [9; 7] has emerged as a promising alternative, decoupling model capacity from computation by leveraging sparsely activated expert subnetworks while maintaining approximately constant active FLOPs. However, since the relationship between loss and sparsity follows a log-linear trend [49], the benefits of expert sparsity also saturate rapidly. Moreover, sparse models also exhibit lower sample efficiency, requiring larger datasets to reach convergence [27; 28], alongside significant engineering challenges to ensure hardware efficiency and low latency [16; 32] for routing balance [25].

Recognizing that scaling dense parameters, data, and expert sparsity all encounter fundamental bottlenecks, in this paper, we explore token-indexed parameters as an orthogonal and complementary scaling dimension. Specifically, we propose a module called Joint-Token (JTok), which augments each Transformer layer by applying a token-specific modulation vector—retrieved from learned embedding tables—to gate the MLP residual [11] via lightweight Hadamard products. Furthermore, we

\*Corresponding author: yanjunchi@sjtu.edu.cn.

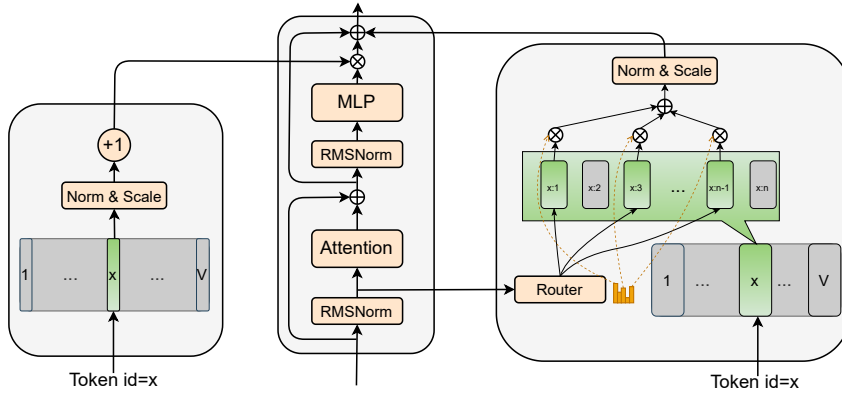


Figure 1: **Architecture of JTOK/JTok-M.** JTOK (left) augments each Transformer layer with a token-indexed table. Each token retrieves a modulation vector, applies norm and a learnable per-dimension scaling, and forms a lightweight multiplicative gate to modulate the FFN update via element-wise products. JTOK-M (right) generalizes JTOK by maintaining a pool of token-indexed modulators and using a router conditioned on the hidden state to select a sparse Top- $K$  mixture per token; the mixed modulator is normalized+scaled and injected as an additional residual alongside the backbone update. Both are plug-in bypass modules implemented with table lookups and element-wise operations, allowing retrieval to be overlapped with backbone and adding negligible compute.

extend JTOK into a sparse variant, Mixture of JTOK (JTOK-M), which maintains a pool of modulators per token and employs a lightweight router to select context-appropriate mixtures.

This architectural design explicitly addresses the bottlenecks inherent in the aforementioned scaling paradigms. First, by relying on element-wise modulation instead of dense matrix multiplications, JTOK injects substantial capacity with minimal FLOPs overhead, thereby overcoming the efficiency limits of dense scaling. Second, unlike standard MoE models that incur high communication and HBM overhead, our retrieval-based mechanism is largely decoupled from the backbone computation. This enables asynchronous prefetching of parameters, which can be overlapped with backbone execution—effectively mitigating the latency typically associated with high sparsity.

Extensive experiments reveal that JTOK-M fundamentally shifts the quality-compute Pareto frontier, delivering consistent performance gains even as the backbone model scale increases. Furthermore, we explicitly validate the scalability of this dimension: the loss exhibits a log-linear trend with the number of token-indexed parameters, confirming that this axis follows a scaling law similar to dense parameters. **To summarize, our contributions are as follows:**

- We introduce token-indexed parameters as a novel scaling axis that expands model capacity without increasing FLOPs, offering a complementary axis to traditional dense and sparse scaling.
- We propose JTOK and JTOK-M, practical architectures that leverage token-indexed modulation to enhance both dense and MoE models with negligible FLOPs overhead.
- We show that JTOK-M consistently accelerates convergence and reduces training loss, directly translating into significant downstream performance gains. Notably, on a large-scale 17B MoE backbone, our approach delivers substantial improvements (e.g., +4.1 on MMLU, +8.3 on ARC, and +8.9 on CEval), validating its robustness in enhancing both data efficiency and model generalization.
- We establish token-indexed parameters as a highly efficient and scalable dimension. Rigorous iso-compute analysis confirms a 35% compute saving that remains stable across backbone scales, while the token-indexed parameters themselves exhibit a predictable log-linear scaling behavior, offering a proven trajectory for future model expansion.
- We propose efficient implementation strategies with which, training throughput loss is less than 7%; for inference, there is no additional GPU memory footprint, with a moderate latency increase of  $\leq 7.3\%$ .

---

## 2 RELATED WORKS

**Scaling Law.** The Kaplan scaling law [23] empirically shows that LLM performance follows power-law with parameters, data, and compute, enabling extrapolation across orders of magnitude. Chin-chilla [15] refined these findings into compute-optimal training prescriptions, arguing that many earlier LLMs were under-trained and that optimal scaling under fixed training compute requires increasing training tokens roughly proportionally with model parameters. [42] incorporate deployment considerations by explicitly accounting for inference cost in the scaling objective, showing that when inference demand is very high, the overall-optimal strategy may favor smaller models trained for longer to minimize end-to-end compute.

In parallel, scaling-law frameworks have been extended to Mixture-of-Experts (MoE) architectures. [27] introduced a granularity hyperparameter for MoE models and found MoE consistently outperforms compute-matched dense models, with gains increasing at larger scales. [49] proposed the efficiency leverage metric and empirically linked efficiency gains to factors such as expert-activation fraction via power laws, predicting that well-configured MoE can match dense performance with substantially less compute. Overall, these works systematize LLM scaling laws across compute allocation, inference cost, and alternative architectures, offering practical guidance for improving efficiency.

**Vocabulary Scaling** emerges as another factor for quality and efficiency. [48] provides a compute-optimal rule indicating that larger models benefit from larger vocabularies and show fixed-FLOPs gains. In continual-training scenarios, [47] replacing the old vocabulary with a better-matched one outperforms keeping the original tokenizer. [17] decouples input/output vocabularies to enlarge only the input side with no extra inference cost; SuperBPE [33] extends BPE with a simple pretokenization curriculum—learn subwords first, then allowing merges across whitespace to form multi-word tokens—improving encoding efficiency and downstream performance. BLT [37] replaces fixed-vocabulary tokens with dynamically sized byte patches as the main computation units, enabling tokenizer-free scaling with improved efficiency and robustness.

*Distinction from our approach:* While existing methods primarily scale the vocabulary dimension  $V$ —often utilizing techniques like hash N-grams [17; 57]—they are inherently constrained by combinatorial limits. Such expansions tend to capture fixed, local surface patterns without deepening semantic understanding. In contrast, we scale along the feature dimension  $d$ , providing a high-dimensional, context-interactive space in which tokens can acquire richer semantics through attention-mediated interactions during training.

**Mixture of Experts.** MoE architectures have advanced toward sparser routing, finer-grained experts, and greater deployability. The sparsely-gated MoE of [43] activates only a small subset of FFN experts per example via a trainable gate with an auxiliary load-balance loss, scaling capacity to tens of billions of parameters with limited extra compute and validating conditional computation for language modeling and translation. Switch Transformer [9] further simplifies routing by selecting a single expert per token, yielding a favorable speed-quality trade-off under fixed compute and enabling trillion-parameter scaling. [7; 31] pushes extreme expert specialization by partitioning experts more finely and isolating shared experts for generic knowledge, improving utilization and reducing redundancy, and reporting competitive or superior performance to larger dense/MoE baselines at comparable cost. To ease deployment and accelerate inference, [21] reparameterizes trained FFN experts into lookup tables for inference, retrieving precomputed expert outputs on demand to slash VRAM usage and avoid real-time expert compute, which yields dense-like latency in their setting.

**Large Memory Layer.** Large memory layers expand model capacity by decoupling parameters from compute. Product Key Memory [29] inserts a very large, sparsely accessed key-value table into the FFN, adding minimal extra FLOPs while improving language modeling at scale. PEER [12] further extends product-key style routing to sparsely select from a pool of over a million tiny experts, improving the performance-compute trade-off in a fine-grained MoE-like regime. Ultra-Sparse Memory [19] introduces an ultra-sparse memory layer that activates only a few memory slots per token and reports reduced inference latency while maintaining performance. Memory Layers at Scale [2] shows that replacing some FFNs with trainable key-value memory layers scales to very large memory capacity and can outperform dense models using substantially more FLOPs, while also being competitive with MoE under matched budgets.

### 3 METHODOLOGY

#### 3.1 PRELIMINARY

##### 3.1.1 PRE-NORM TRANSFORMER BLOCK

We adopt the Pre-Norm Transformer [52] as our backbone, a prevalent architecture in current SOTA open-source models [56; 32] due to its robustness in stabilizing training dynamics and gradients [60]. In this setting, each sub-module operates on a normalized hidden state and contributes an additive residual update. Concretely, for token  $x$  at layer  $\ell$ ,

$$\Delta \mathbf{a}_x^\ell = \text{Attn}^\ell(\text{RMSNorm}(\mathbf{h}_x^\ell)), \quad (1)$$

$$\tilde{\mathbf{h}}_x^\ell = \mathbf{h}_x^\ell + \Delta \mathbf{a}_x^\ell, \quad (2)$$

$$\Delta \mathbf{m}_x^\ell = \text{FFN}^\ell(\text{RMSNorm}(\tilde{\mathbf{h}}_x^\ell)), \quad (3)$$

$$\mathbf{h}_x^{\ell+1} = \tilde{\mathbf{h}}_x^\ell + \Delta \mathbf{m}_x^\ell, \quad (4)$$

where  $\text{FFN}^\ell(\cdot)$  is the MLP for dense model and becomes sparsely-activated experts for MoE.

##### 3.1.2 SCALING LAWS AND ISOFLOP PROFILES

**Scaling Law Form.** Neural scaling laws provide an empirical yet principled lens through which to reason about the quality-compute trade-off of LLM training. According to the Kaplan scaling law [23], the test loss can be modeled as:

$$\mathcal{L}(N_c, D) = \left[ \left( \frac{A}{N_c} \right)^{\frac{\alpha}{\beta}} + \frac{B}{D} \right]^{\beta}, \quad (5)$$

where  $N_c$  denotes the compute-intensive parameters (in MoE cases, it refers to activated parameters), excluding both embedding and LM prediction head;  $D$  is the number of training tokens, and  $A, B, \alpha, \beta$  are empirical constants.

**IsoFLOPs Profiles.** IsoFLOPs profiles provide an empirical procedure for estimating the compute-optimal allocation between model size and data under a fixed training FLOPs budget [15]. Under standard Transformer FLOPs accounting, training a model with  $N_c$  compute-intensive parameters<sup>1</sup> for  $D$  tokens costs approximately  $C \approx 6N_c D$  FLOPs [38]. The compute-optimal loss at budget  $C$  is defined as

$$\mathcal{L}^*(C) = \mathcal{L}(N_c, D), \quad s.t. \quad 6N_c D = C \quad (6)$$

To estimate  $\mathcal{L}^*(C)$  in practice, a set of target budgets  $\{C_i\}$  is fixed. For each  $C_i$ , model size  $N_c$  is swept over a grid, and the corresponding token budget is set to  $D = C_i/(6N_c)$  so that each run matches the same total FLOPs. After training, the final held-out loss is recorded for each configuration, yielding an IsoFLOPs curve of loss versus  $N_c$  at constant  $C_i$ , which typically exhibits a U-shaped profile with a clear minimum. A quadratic fit around the valley can be used to estimate the loss-optimal model size  $N_c^*(C_i)$  and token count  $D^*(C_i)$  for each budget. Collecting minima across budgets forms the empirical efficient frontier  $\{(C_i, \mathcal{L}^*(C_i))\}$ .

### 3.2 JTOK

JTok scales the token embedding along hidden dimension  $d$ . As illustrated in Fig. 1 (left), every transformer layer  $\ell$  keeps a learnable table  $\mathbf{E}^\ell \in \mathbb{R}^{V \times d}$ . Each token retrieves a vector  $\mathbf{E}^\ell[x]$  with its ID  $x \in [V]$  and gates the backbone module’s residual updates via Hadamard products.

**Mechanism.** Let  $x$  be the token id,  $\Delta \mathbf{m}_x^\ell$  be the MLP module increments. JTOK forms multiplicative gate  $\mathbf{p}_x^\ell \in \mathbb{R}^d$ :

$$\mathbf{p}_x^\ell = \mathbf{1} + \mathbf{s}^\ell \odot \text{Norm}_\varepsilon(\mathbf{E}^\ell[x]), \quad (7)$$

<sup>1</sup>Here, the parameters consist of attention qkvo matrices and mlp parameters (or activated experts for MoE).

---

where  $\mathbf{s}^\ell \in \mathbb{R}^d$  is a learnable per-dimension scaler and  $\text{Norm}_\varepsilon(\mathbf{u}) = \frac{\mathbf{u}}{\|\mathbf{u}\|_2 + \varepsilon}$  ( $\varepsilon$  is a small constant to avoid division by zero). We empirically validate the effectiveness of this normalization term in Appendix D.2. The gated MLP increments is

$$\Delta \hat{\mathbf{m}}_x^\ell = \Delta \mathbf{m}_x^\ell \odot \mathbf{p}_x^\ell, \quad (8)$$

which then adds to the backbone residual:

$$\mathbf{h}_x^{\ell+1} = \tilde{\mathbf{h}}_x^\ell + \Delta \hat{\mathbf{m}}_x^\ell. \quad (9)$$

### 3.3 MIXTURE OF JTOK (JTOK-M)

To further unlock the potential of token-indexed parameters, we introduce JTOK-M. JTOK-M generalizes from a static mapping to a dynamic, context-aware routing framework. By maintaining a larger pool of modulators and leveraging the hidden state as a contextual signal to guide the selection, JTOK-M adaptively selects a sparse mixture of parameters for each token instance. This design enables the model to capture context-dependent semantics and significantly expands the parameter space while preserving the efficiency of sparse retrieval. As shown in Fig. 1 (right).

**Mechanism.** Each token is equipped with a pool of  $n_e$  modulators per layer and uses a router to pick top- $K$  of them given the hidden state.

Formally, for token  $x$ , let  $\text{RMSNorm}(\mathbf{h}_x^\ell)$  be the input of attention in layer  $\ell$ . Each layer maintains a pool  $\{\mathbf{E}_i^\ell \in \mathbb{R}^{V \times d}\}_{i=1}^{n_e}$ . A linear router computes logits

$$\mathbf{g}_x^\ell = (\text{RMSNorm}(\mathbf{h}_x^\ell))^\top \mathbf{R}^\ell \in \mathbb{R}^{n_e}, \quad \mathbf{R}^\ell \in \mathbb{R}^{d \times n_e}, \quad (10)$$

selects  $G_x^\ell = \text{TopK}(\mathbf{g}_x^\ell, K)$ , and forms normalized weights  $w_i^\ell = \frac{\sigma(g_i^\ell)}{\sum_{j \in G_x^\ell} \sigma(g_j^\ell)}$  for  $i \in G_x^\ell$  with a Sigmoid  $\sigma$  [36]. The mixed token-indexed vector is:

$$\mathbf{e}_x^\ell = \sum_{i \in G_x^\ell} w_i^\ell \mathbf{E}_i^\ell[x] \in \mathbb{R}^d. \quad (11)$$

We normalize and apply a learnable element-wise scaler  $\mathbf{s}_{\text{JTOK-M}}^\ell \in \mathbb{R}^d$ , producing the additive residual injection. To ensure the variance of the hidden states controllable [39], we scale with an extra factor  $\frac{1}{\sqrt{2N_l}}$ , where  $N_l$  is the number of layers of the backbone. The ablation of this scaling factor is provided in Appendix D.1.

$$\Delta \mathbf{r}_x^\ell = \frac{1}{\sqrt{2N_l}} \cdot \mathbf{s}_{\text{JTOK-M}}^\ell \odot \text{Norm}_\varepsilon(\mathbf{e}_x^\ell), \quad (12)$$

Finally,  $\Delta \mathbf{r}_x^\ell$  is fused into the layer write-back together with MLP output  $\Delta \mathbf{m}_x^\ell$ :

$$\mathbf{h}_x^{\ell+1} = \tilde{\mathbf{h}}_x^\ell + \Delta \mathbf{m}_x^\ell + \Delta \mathbf{r}_x^\ell \quad (13)$$

To encourage all the embedding experts to be adequately utilized and trained, we incorporate an auxiliary load-balancing loss during training, similar to standard practice in MoE models. Implementation details are provided in Appendix B.

### 3.4 SYSTEM EFFICIENCY

Token-indexed parameters shift the main system concern from GEMMs to parameter access and memory footprint. While the Transformer backbone is typically compute-bound, token-indexed modules have negligible FLOPs but are dominated by memory access. Accordingly, our system design targets:

1. keeping token-indexed access off the GEMM critical path by overlapping retrieval with backbone compute via asynchronous prefetch/overlap (Sec. 3.4.3), and minimizing memory traffic via token deduplication (Sec. 3.4.2);
2. reducing the HBM footprint of token-indexed tables via embedding model parallelism (Sec. 3.4.4) and CPU offloading (Sec. 3.4.5).

These strategies allow JTOK/JTok-M to scale to massive memory capacities with minimal impact on efficiency.

---

### 3.4.1 COMPUTATIONAL COMPLEXITY ANALYSIS

Per token and per layer, JTok adds a normalization, a Hadamard product for gating, and a residual write-back, all of which are  $\mathcal{O}(d)$ .<sup>2</sup>

JTok-M additionally computes router logits and mixes top- $K$  modulators. Routing is a single matrix-multiply with cost  $\mathcal{O}(dn_e)$ , and mixture application is  $\mathcal{O}(Kd)$ . In practice  $n_e$  and  $K$  are small constants, so the overall overhead remains linear in  $d$  and is negligible compared to the backbone’s  $\Theta(d^2)$  attention/FFN computes.

### 3.4.2 MEMORY ACCESS AND ZIPFIAN PATTERNS

The dominant overhead of JTok/JTok-M is memory traffic from table lookups. For each layer, JTok reads  $d$  elements per token, while JTok-M reads  $Kd$ . However, token frequencies follow a Zipfian distribution [61], so high-frequency tokens are repeatedly accessed. This enables *token deduplication*: unique token ids in a micro-batch are gathered once and then scattered back to all occurrences, avoiding redundant reads.

### 3.4.3 DECOUPLING AND ASYNCHRONOUS OVERLAP

JTok/JTok-M are bypass modules, decoupled from backbone, so their execution can be scheduled independently of attention/FFN computation, enabling overlapping memory access with compute. Concretely, embedding gathers for some layer can be issued asynchronously while the backbone executes GEMMs for the current layer, and the retrieved vectors are fused only at the layer write-back (Eqs. equation 9 and equation 13). As a result, a substantial portion of the retrieval latency can be hidden under compute, making the end-to-end throughput impact small in practice.

### 3.4.4 EMBED-PARALLEL IN TRAINING

Token-indexed tables are large but sparsely accessed, making them well-suited for *embedding model parallelism*. Tables can be sharded across GPUs, reducing per-device memory footprint, allowing larger micro-batches and increasing training throughput. For JTok, the cross-device communication per token is  $d$  elements. For JTok-M, a naive implementation would communicate  $Kd$  elements, but this can be avoided by *owner-rank premixing*: the device that owns the selected modulators performs the weighted sum locally, and only the mixed vector ( $d$ -sized) is communicated.

### 3.4.5 CPU OFFLOADING IN INFERENCE

Since token-indexed parameters are accessed sparsely, the host-to-device transfer volume depends on the number of requested vectors, not on the full table size. Per layer, transferring the retrieved values scales as  $\mathcal{O}(d)$  for JTok and  $\mathcal{O}(Kd)$  for JTok-M, independent of  $V$  and of the overall parameter capacity stored on the host. This property makes CPU offloading a practical option during inference to save HBM usage. Specifically, the tables can reside in CPU memory, while only the small set of vectors needed by the current batch are streamed to GPUs and overlapped with backbone execution.

## 3.5 SCALING HYPOTHESIS OF TOKEN-INDEXED PARAMETERS

Building on the Kaplan scaling law (Eq. 5) and the FLOPs constraint  $C \approx 6N_cD$  introduced in the Preliminary, we introduce one core assumption: effective parameter count  $N_{\text{eff}}$ . This assumption integrates token-indexed parameters into the scaling law and yields a *scale-invariant* isoperformance compute saving in the compute-optimal regime.

**Core assumption: effective parameters  $N_{\text{eff}}$ .** We denote the backbone compute-intensive parameters as  $N_c$  and the token-indexed parameters as  $N_n$ . Let  $\eta \triangleq N_n/N_c$  be the parameter expansion ratio. JTok-M retrieves and injects token-indexed vectors per token and per layer; its usable capacity depends on routing sparsity. We capture this with a JTok-M architecture-dependent discount function  $\gamma(\rho)$ , where  $\rho$  denotes the JTok-M activation sparsity ( $\rho = K/n_e$ ). We define

$$N_{\text{eff}} \triangleq N_c + \gamma(\rho)N_n = N_c(1 + \eta\gamma(\rho)). \quad (14)$$

---

<sup>2</sup>From the roofline [54] perspective, these element-wise Ops could be limited by memory traffic and kernel-launch. Kernel fusion can amortize launches and avoid extra memory round-trips.

Importantly,  $N_{\text{eff}}$  characterizes *effective capacity*, whereas the dominant training FLOPs are still governed by  $N_c$ ,  $D$ .

**Incorporating  $N_{\text{eff}}$  into the Kaplan scaling law.** Starting from Eq. 5, we replace the  $N_c$  with  $N_{\text{eff}}$ :

$$\mathcal{L}_{\text{JTOK-M}}(N_c, D; \eta, \rho) = \left[ \left( \frac{A_{\text{JTOK-M}}}{N_c} \right)^{\frac{\alpha}{\beta}} + \frac{B}{D} \right]^{\beta}, \quad (15)$$

where  $A_{\text{JTOK-M}} \triangleq A/(1 + \eta\gamma(\rho))$ . This highlights that JTOK-M is equivalent to rescaling the constant in the model-size term, while leaving the data term  $B/D$  and the dominant FLOPs form unchanged.

**Isoperformance compute saving under compute-optimal training.** Let  $\mathcal{L}^*(C)$  denote the compute-optimal efficient frontier of backbone model defined in Eq. 6. Similarly, the JTOK-M compute-optimal frontier becomes a *multiplicative downward shift*:

$$\mathcal{L}_{\text{JTOK-M}}^*(C; \eta, \rho) = (1 + \eta\gamma(\rho))^{-\frac{\alpha\beta}{\alpha+\beta}} \cdot \mathcal{L}^*(C). \quad (16)$$

Together, for any target test loss  $\mathcal{L}^*$ , the minimal compute required satisfies

$$C_{\text{JTOK-M}}^*(\mathcal{L}^*) = \frac{1}{1 + \eta\gamma(\rho)} C_{\text{base}}^*(\mathcal{L}^*). \quad (17)$$

The key insight of Eq. 17 is that the **compute saving ratio is independent of the backbone scale** and depends only on JTOK-M architectural hyperparameters (e.g.,  $\eta$ ,  $\rho$ , and  $\gamma(\cdot)$ ). The detailed derivations of Eq. 16 and Eq. 17 are provided in Appendix A.

## 4 EXPERIMENTS

### 4.1 MAIN QUALITY RESULTS

#### 4.1.1 EXPERIMENTAL SETUP

We first validate that token-indexed parameters consistently improve quality across diverse architectures (including both dense and MoE models) and backbone scales (up to 17B), before examining scaling behaviors and efficiency.

**Backbone Models.** We establish backbone using both dense and MoE architectures. For dense models, we use four Qwen-style [55] models of varying sizes: 190M(S), 0.5B(M), 1B(L), and 1.5B(XL) parameters. For MoE models, we use two highly-sparse configurations: one with 250M activated parameters and 1.5B total parameters (1.5B-A250M), and another with 0.5B activated parameters and 3.2B total parameters (3.2B-A0.5B). Each MoE layer contains 145 experts, with one shared expert [7] and 144 routed experts, from which the top-8 are activated per token. To further investigate the scalability of our approach on large-scale foundation models, we introduce a 17B MoE backbone (17B-A2B). This model features 28 layers with 65 experts (1 shared expert) per layer, activating top-6 per token, resulting in 1.9B activated parameters. For more details about the model configurations, please refer to Appendix E.

**JTok/JTok-M Configuration.** We evaluate two methods: JTOK and JTOK-M. Both are implemented as attached modules that augment the backbone model without modifying its architecture. JTOK is benchmarked on the dense-XL, the 1.5B-A250M MoE and the 3.2B-A0.5B MoE backbones. JTOK-M is evaluated on the 1.5B-A250M, the 3.2B-A0.5B and the 17B-A2B MoE backbones. For JTOK-M, we set the number of modulator experts  $n_e = 5$  and activate the top  $K = 2$ . See Appendix E for detail of the additional parameter counts introduced by the JTOK and JTOK-M modules.

**Datasets and Training.** All models are pretrained with Megatron-LM framework [44]. The S, M, and L dense models are pretrained for 100B tokens on the Fineweb-edu [35], an open-source collection of text dataset. The XL dense model and all MoE models are trained on another high-quality dataset curated from online corpora, which includes general text, code, math, and multilingual content after rigorous filtering. Both XL dense and 1.5B-A250M MoE are trained for 300B tokens, and the 3.2B-A0.5B MoE for 500B tokens. The 17B MoE backbone and its JTOK-M variant are trained for 570B tokens on the same high-quality curated dataset. All training configurations for the

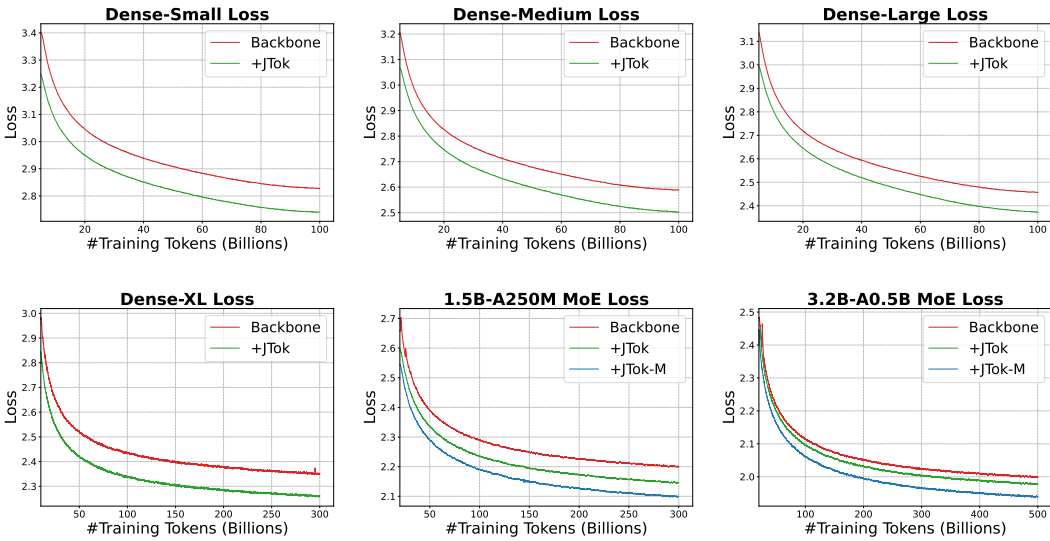


Figure 2: **Training loss for dense and MoE backbones and corresponding JTOK and JTOK-M variants.** The top row shows JTOK’s performance on Dense-S(190M), M(505M), and L(1B) backbones. The bottom row shows results on Dense-XL (1.5B), 1.5B-A250M MoE, and 3.2B-A0.5B MoE backbones. In all settings, JTOK (and JTOK-M for MoE backbone) achieves a consistently and significantly lower training loss.

JTok and JTOK-M models are kept identical to those of their corresponding backbones. For detailed training hyperparameters, see Appendix E.

**Evaluation.** We evaluate downstream benchmark performances of dense-XL, 1.5B-A250M and 3.2B-A0.5B MoEs as well as corresponding JTOK/JTOK-M variants using OpenCompass [6] framework. The downstream benchmarks distribute in 4 domains: *Knowledge* (MMLU [13], TriviaQA [22], ARC [4], GPQA [40]), *Reasoning* (Hellaswag [58], C3 [45], BBH [46], SocialIQA [41]), *Code* (MBPP [1], HumanEval [3], LiveCodeBench [20]) and *Math* (MATH [14], GSM8K [5], DROP [8]).

Additionally, for the 17B-A2B MoE and its JTOK-M variant (17B + 44B embedding), we track the accuracy trajectories against the number of training tokens on six representative benchmarks: MMLU, ARC, Hellaswag, and CMMLU [30], CEval [18], Xiezhi [10] to analyze the convergence behavior and performance scaling dynamics.

#### 4.1.2 RESULTS AND ANALYSIS

**Training Loss.** As shown in Fig. 2, our proposed methods achieve a consistent and significant reduction in training loss across all model scales and architectures. For the dense models, JTOK consistently maintains a lower loss trajectory. Similarly, for the MoE models, both JTOK and JTOK-M show a clear advantage over the vanilla backbones, reducing the training loss for both the 1.5B and 3.2B MoE configurations. This shows that JTOK and JTOK-M are robust methods for improving optimization and data compression.

**Downstream Performance.** The benefits observed during training translate to significant and consistent improvements in downstream tasks. As shown in Table 1, JTOK boosts the Dense-XL average accuracy from 22.22 to 26.54 (+4.32), with sizable gains on key benchmarks such as MMLU (+4.55) and TriviaQA (+9.50). For MoE, gains are further amplified by JTOK-M (Table 1). On 1.5B-A250M, the average accuracy improves from 18.87 to 22.78 (+3.91); on 3.2B-A0.5B, it rises from 26.75 to 32.34 (+5.59), including strong improvements on ARC-C (+7.25) and GSM8K (+6.31).

Crucially, these gains scale effectively to the large-scale 17B-A2B MoE backbone. As illustrated in Fig. 3, JTOK-M delivers substantial boosts across diverse domains, particularly in knowledge-

Table 1: **Performance evaluation on comprehensive downstream tasks (Knowledge, Code, Reasoning, and Math).** The number in parentheses after each benchmark indicates the number of few-shot examples used in evaluation. B.O. denotes backbone-only; +JTOK and +JTOK-M denote the same backbone augmented with the corresponding plugin. Overall Avg is the mean over all 14 tasks. The best result of each task (within the same backbone block) is highlighted in bold.

Task	1.5B (Dense)		1.5B-A250M (MoE)			3.2B-A0.5B (MoE)		
	B.O.	+JTOK	B.O.	+JTOK	+JTOK-M	B.O.	+JTOK	+JTOK-M
<b>Knowledge</b>								
MMLU(5)	32.74	<b>37.29</b>	27.91	30.98	<b>34.07</b>	36.39	40.05	<b>43.47</b>
TriviaQA(5)	25.72	<b>35.22</b>	22.81	27.31	<b>36.53</b>	39.57	41.13	<b>46.29</b>
ARC-C(25)	35.74	<b>41.58</b>	29.21	30.24	<b>34.72</b>	39.76	43.87	<b>47.01</b>
GPQA(5)	25.60	<b>29.80</b>	25.59	28.28	<b>30.03</b>	29.47	28.79	<b>31.70</b>
<b>Code</b>								
MBPP(3)	9.53	<b>12.20</b>	7.00	10.60	<b>12.50</b>	19.20	21.80	<b>24.51</b>
HumanEval(0)	9.15	<b>9.76</b>	<b>10.57</b>	9.96	10.55	16.46	18.90	<b>19.89</b>
LCB(5)	0.87	<b>2.61</b>	1.57	1.45	<b>1.64</b>	2.52	4.70	<b>5.96</b>
<b>Reasoning</b>								
Hellaswag(10)	51.19	<b>55.07</b>	45.70	48.01	<b>52.06</b>	57.05	58.52	<b>60.37</b>
C3(3)	39.34	<b>47.83</b>	27.95	29.86	<b>30.22</b>	36.84	44.05	<b>49.01</b>
BBH(3)	21.04	<b>24.12</b>	18.96	18.82	<b>20.66</b>	21.87	24.74	<b>28.58</b>
SocialIQA(5)	41.64	<b>45.97</b>	34.44	36.39	<b>38.51</b>	42.63	44.83	<b>47.15</b>
<b>Math</b>								
MATH(4)	2.17	<b>3.36</b>	1.96	3.04	<b>4.37</b>	7.16	8.30	<b>10.42</b>
GSM8K(4)	5.76	<b>9.07</b>	3.87	<b>4.17</b>	4.15	13.65	16.38	<b>19.96</b>
DROP(3)	10.55	<b>17.71</b>	6.60	7.99	<b>8.90</b>	11.86	13.27	<b>18.44</b>
<b>Overall Avg.</b>	22.22	<b>26.54</b>	18.87	20.51	<b>22.78</b>	26.75	29.24	<b>32.34</b>

intensive and reasoning benchmarks—ranging from +4.11 on MMLU to an impressive +9.34 on CMMLU and +8.28 on ARC-C—validating the method’s efficacy on foundation-scale models.

**Training Dynamics.** Beyond final metrics, the accuracy trajectories on the 17B backbone (Fig. 3) reveal a distinct convergence advantage. JTOK-M establishes a performance lead in the early training stage and widens this gap throughout the 570B-token course without saturation. Unlike techniques that only refine convergence at the tail end, token-indexed modulation provides a consistent capacity expansion, allowing the model to absorb complex semantics more efficiently from the onset. This confirms that token-indexed parameters function as an orthogonal scaling dimension that fundamentally elevates the model’s learning capability and data efficiency.

## 4.2 SCALING LAWS

This subsection studies JTOK-M scalability along two axes: (i) whether JTOK-M’s gains remain stable as the backbone scales, which is crucial for applying this feature in real-world LLMs; and (ii) what scaling behavior does it exhibit if scaling JTOK-M itself. Together, these results characterize token-indexed parameters as a predictable and complementary scaling dimension.

### 4.2.1 JTOK-M IS SCALABLE TO LARGE BACKBONES

#### Large-scale Pretrain.

We train both MoE and +JTOK-M variant with three backbone sizes (2.3B-A0.5B, 3.9B-A0.6B, and A9.8B-A1.4B) under a fixed JTOK-M configuration  $(\eta, \rho) = (50, 0.25)$  for 100B tokens.

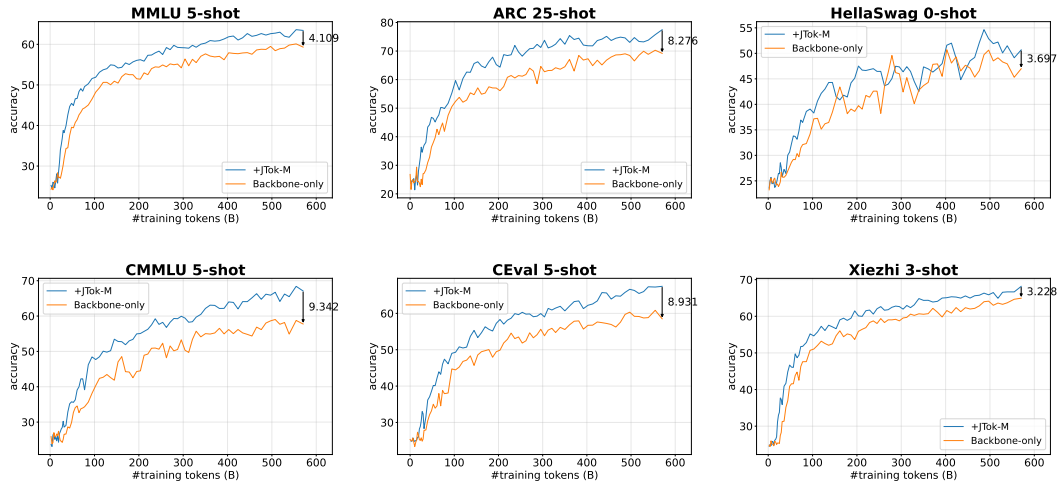


Figure 3: **Downstream accuracy trajectories on the 17B-A2B MoE backbone.** We track the zero/few-shot performance on six representative benchmarks (MMLU, ARC-C, HellaSwag, CMMLU, C-Eval, and Xiezhi) throughout the 570B-token pretraining course. JTok-M (blue) consistently surpasses the backbone baseline (orange) from the early stages, yielding substantial gains in both knowledge-intensive and reasoning tasks without saturation.

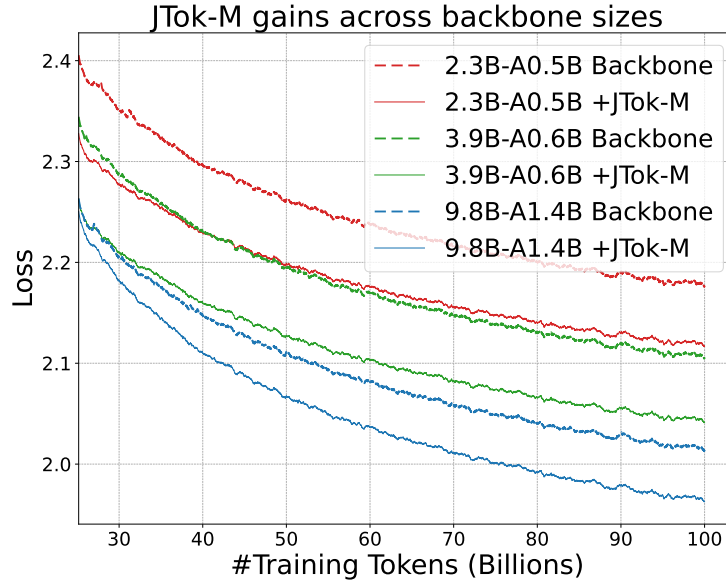


Figure 4: JTok-M (fixed  $(\eta, \rho)$ ) improvements remain stable and consistent across different backbone model sizes.

Fig. 4 shows that JTok-M’s benefits are remarkably consistent across model scales. JTok-M reduces the final loss by 0.059 on the 2.3B-A0.5B backbone, by 0.064 on the 3.9B-A0.6B backbone, and by 0.051 on the A9.8B-A1.4B backbone, corresponding to relative improvements of **2.7%**, **3.0%**, and **2.55%**, respectively.

#### Rigorous IsoFLOPs Validation

In Sec. 3.5, we predict that token-indexed parameters yield a *scale-invariant* improvement under compute-optimal training: across compute budgets, the efficient frontier is shifted downward by a constant multiplicative factor (Eq. 16). Here we demonstrate the validity of this hypothesis via isoFLOPs experiments.

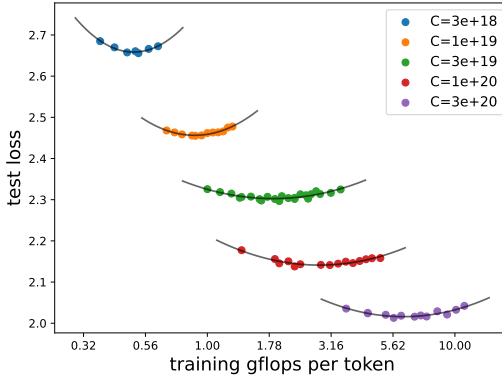


Figure 5: **IsoFLOPs profile of vanilla MoE models.** Each curve shows test loss vs. per-token gFLOPs at fixed FLOPs, with optimal points defining the efficient frontier.

Following the isoFLOPs protocol described in Sec. 3.1.2, we establish the efficient frontier for MoE (top-8 routing, one shared expert, and 145 total experts). We choose five FLOPs budgets that are log-uniformly spaced,  $C \in \{3e18, 1e19, 3e19, 1e20, 3e20\}$ , and then fit a quadratic around the minimum of the resulting U-shaped curve to obtain the compute-optimal configuration  $(N_c^*(C), D^*(C))$  and its best held-out loss  $\mathcal{L}^*(C)$ , as shown in Fig. 5.

For each compute-optimal backbone configuration, we attach the JTok-M module while keeping the backbone architecture and training setup unchanged. JTok-M adds token-indexed parameters but does not change the dominant FLOPs. We use a fixed JTok-M configuration with parameter expansion ratio  $\eta = N_n/N_c = 50$  and activation sparsity  $\rho = 0.25$ . This yields another set of efficient-frontier points  $\{(C, \mathcal{L}_{\text{JTOK-M}}^*(C))\}$  corresponding to JTok-M architecture.

Across all budgets, JTok-M improves the compute-optimal loss, and the improvement is well-approximated by a constant multiplicative factor, consistent with Eq. 16. To make the comparison explicit, we analyze the frontiers in log-log space. Taking logarithms of Eq. 16 gives

$$\log \mathcal{L}_{\text{JTOK-M}}^*(C; \eta, \rho) = \log \mathcal{L}^*(C) - \frac{\alpha\beta}{\alpha + \beta} \log(1 + \eta\gamma(\rho)) \quad (18)$$

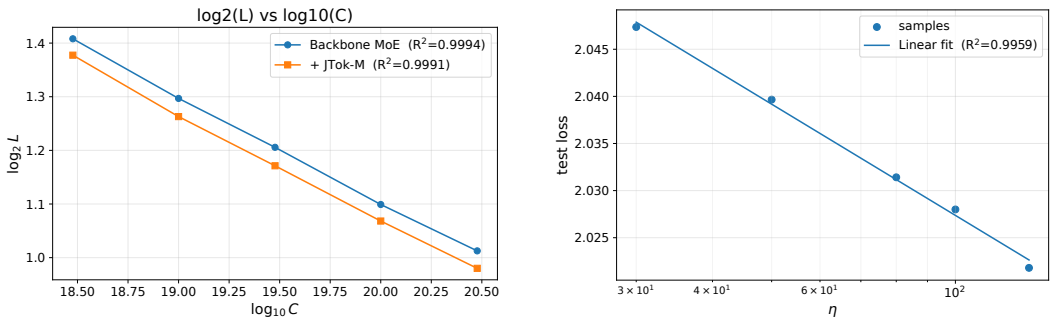
which predicts that the vertical gap between the two frontiers in log space is  $C$ -invariant and depends solely on the JTok-M hyperparameters through  $(\eta, \rho)$ . Empirically, linear fits of  $\log \mathcal{L}^*(C)$  and  $\log \mathcal{L}_{\text{JTOK-M}}^*(C)$  versus  $\log C$  yield nearly identical slopes, while JTok-M exhibits a clear downward intercept shift, as shown in Fig. 6a. This verifies that JTok-M improves the quality-compute Pareto frontier in a manner that is stable across scales. Quantitatively, under matched compute budgets, JTok-M achieves a consistent **2.2% loss reduction**; equivalently, to reach any target test loss, JTok-M **saves 35% compute** relative to MoE. Detailed regression statistics and the mathematical derivation of the compute saving ratio are provided in Appendix C.

#### 4.2.2 SCALING JTOK-M ITSELF

In subsection 4.2.1, we validate that JTok-M can be reliably applied to larger backbone as its relative gains remain stable under large-scale pretraining, and the rigorous IsoFLOPs study verifies a scale-invariant downward shift of the compute-optimal frontier. We now examine the complementary question: *can JTok-M itself be scaled as a standalone capacity axis, and does it exhibit a predictable scaling behavior?*

**Experimental Setup.** We fix the backbone to a single MoE model (3.9B-A0.6B) and pretrain for 100B tokens. On top of this frozen backbone specification, we attach JTok-M modules of varying capacity. Concretely, we parameterize the JTok-M size using the parameter expansion ratio  $\eta$ ; We sweep  $\eta$  from 30 to 130 while fixing the sparsity ratio  $\rho = 0.25$ . All other JTok-M hyperparameters and all training hyperparameters are kept identical across runs, so that the observed differences are attributable solely to scaling  $N_n$ .

**Results** Fig. 6b shows that increasing JTok-M capacity leads to a clear and consistent reduction in held-out loss. Within the explored range, the improvement is monotonic with no sign of degradation,



(a) **Efficient frontiers of MoE and +JTok-M variant.** JTok-M achieves 2.2% lower loss at each compute budget, equivalent to saving 35% compute to reach each test loss.

(b) **Scaling behavior of JTok-M.** The validation loss follows an approximately log-linear trend with respect to the JTok-M parameter expansion ratio  $\eta$ .

Figure 6: JTok-M improves the efficient frontier and follows a log-linear scaling trend with  $\eta$ .

Table 2: Training throughput (tokens/s) on the 3.2B-A0.5B MoE backbone with JTok-M ( $\eta = 50$ ). EmbP denotes embedding parallel, and Dedup denotes token deduplication.

Model	Throughput (tok/s)
Baseline	4,838K
JTok-M (naive)	2,749K
JTok-M (EmbP)	4,024K
JTok-M (EmbP+Dedup)	4,510K (-6.78%)

Table 3: Inference throughput on  $8 \times H800$  using SGLang (batch size=16, sequence length=4K) on the 3.2B-A0.5B MoE backbone. JTok/JTok-M use CPU offloading for token-indexed tables.

Model	Prefill (tok/s)	Decode (tok/s)
Baseline	363.7K	4494
JTok (CPU-offload)	360.8K (-0.8%)	4290 (-4.5%)
JTok-M (CPU-offload)	355.2K (-2.3%)	4166 (-7.3%)

indicating that JTok-M provides an effective capacity knob beyond backbone scaling. Moreover, the trend is well-approximated by a smooth power law (linear in log-space): each doubling of JTok-M parameters reduces the loss by approximately **0.0118**. This provides evidence that token-indexed parameters form an orthogonal scaling axis that introduces negligible backbone compute.

#### 4.3 SYSTEM EFFICIENCY

We evaluate the end-to-end training and inference efficiency of JTok/JTok-M. With sufficient system optimizations, the throughput drop of JTok/JTok-M can be bounded within 6.78% for training and 7.3% for inference, demonstrating that JTok/JTok-M is practical for both large-scale training and deployment.

**Experimental Setup.** (1) Training. We measure pretraining throughput (tokens/s) on  $128 \times H800$ , with batch size 1024 and sequence length 8192, on the 3.2B-A0.5B MoE backbone. For JTok-M, we set  $\eta = 50$  and  $\rho = 0.25$ . We compare (i) backbone-only, (ii) +JTok-M without optimization, (iii) +JTok-M with embedding parallelism, and (iv) +JTok-M with embedding parallelism plus token deduplication.

(2) Inference. We benchmark inference on  $8 \times H800$  with batch size 16 and sequence length 4K using SGLang [59]. We implement CPU-offloaded JTok/JTok-M and report prefill and decode throughput on the 3.2B-A0.5B MoE backbone.

---

**Results.** Table 2 shows that a naive JTok-M implementation reduces training throughput mainly for two reasons: (i) the additional memory lookup and (ii) the token-indexed parameters increasing HBM usage, forcing a smaller micro-batch and lower MFU. Embedding parallelism alleviates the latter by sharding tables across GPUs to reduce per-device memory footprint, while token deduplication addresses the former by removing repeated gathers for frequent token access. With joint optimizations, the training throughput reduction is controlled within 6.78%.

Table 3 shows that CPU-offloaded JTok/JTok-M incurs only small inference overhead. Prefill throughput drops by 0.8% (JTok) and 2.3% (JTok-M), while decode drops by 4.5% and 7.3%, respectively. This is expected as decode is more compute-light than prefill, leaving less backbone computation to overlap and hide the host-to-device transfer latency. Overall, the throughput reduction remains low, supporting practical deployment.

## 5 CONCLUSION AND OUTLOOK

We have established token-indexed parameters as a novel and complementary scaling axis for large language models. Our proposed architectures, JTok and JTok-M, consistently enhance both dense and MoE models with negligible system overhead. Extensive evaluations show that our methods significantly boost performance across a wide range of downstream tasks.

Rigorous isoFLOPs analysis confirms that JTok-M fundamentally shifts the quality-compute Pareto frontier, achieving baseline-matching performance with 35% compute savings. Furthermore, we empirically show that token-indexed parameter itself exhibits a predictable power-law scaling behavior, establishing this dimension as a robust and scalable trajectory for future LLM advancement.

---

## REFERENCES

- [1] Jacob Austin, Augustus Odena, Maxwell Nye, Maarten Bosma, Henryk Michalewski, David Dohan, Ellen Jiang, Carrie Cai, Michael Terry, Quoc Le, et al. Program synthesis with large language models. *arXiv preprint arXiv:2108.07732*, 2021.
- [2] Vincent-Pierre Berges, Barlas Oğuz, Daniel Haziza, Wen-tau Yih, Luke Zettlemoyer, and Gargi Ghosh. Memory layers at scale. *arXiv preprint arXiv:2412.09764*, 2024.
- [3] Mark Chen, Jerry Tworek, Heewoo Jun, Qiming Yuan, Henrique Ponde De Oliveira Pinto, Jared Kaplan, Harri Edwards, Yuri Burda, Nicholas Joseph, Greg Brockman, et al. Evaluating large language models trained on code. *arXiv preprint arXiv:2107.03374*, 2021.
- [4] Peter Clark, Isaac Cowhey, Oren Etzioni, Tushar Khot, Ashish Sabharwal, Carissa Schoenick, and Oyvind Tafjord. Think you have solved question answering? try arc, the ai2 reasoning challenge. *arXiv preprint arXiv:1803.05457*, 2018.
- [5] Karl Cobbe, Vineet Kosaraju, Mohammad Bavarian, Mark Chen, Heewoo Jun, Lukasz Kaiser, Matthias Plappert, Jerry Tworek, Jacob Hilton, Reiichiro Nakano, et al. Training verifiers to solve math word problems. *arXiv preprint arXiv:2110.14168*, 2021.
- [6] OpenCompass Contributors. Opencompass: A universal evaluation platform for foundation models. <https://github.com/open-compass/opencompass>, 2023.
- [7] Damai Dai, Chengqi Deng, Chenggang Zhao, RX Xu, Huazuo Gao, Deli Chen, Jiashi Li, Wangding Zeng, Xingkai Yu, Yu Wu, et al. Deepseekmoe: Towards ultimate expert specialization in mixture-of-experts language models. *arXiv preprint arXiv:2401.06066*, 2024.
- [8] Dheeru Dua, Yizhong Wang, Pradeep Dasigi, Gabriel Stanovsky, Sameer Singh, and Matt Gardner. Drop: A reading comprehension benchmark requiring discrete reasoning over paragraphs. *arXiv preprint arXiv:1903.00161*, 2019.
- [9] William Fedus, Barret Zoph, and Noam Shazeer. Switch transformers: Scaling to trillion parameter models with simple and efficient sparsity. *Journal of Machine Learning Research*, 23(120):1–39, 2022.
- [10] Zhouhong Gu, Xiaoxuan Zhu, Haoning Ye, Lin Zhang, Jianchen Wang, Yixin Zhu, Sihang Jiang, Zhuozhi Xiong, Zihan Li, Weijie Wu, et al. Xiezhi: An ever-updating benchmark for holistic domain knowledge evaluation. In *Proceedings of the AAAI conference on artificial intelligence*, volume 38, pp. 18099–18107, 2024.
- [11] Kaiming He, Xiangyu Zhang, Shaoqing Ren, and Jian Sun. Deep residual learning for image recognition. In *Proceedings of the IEEE conference on computer vision and pattern recognition*, pp. 770–778, 2016.
- [12] Xu Owen He. Mixture of a million experts. *arXiv preprint arXiv:2407.04153*, 2024.
- [13] Dan Hendrycks, Collin Burns, Steven Basart, Andy Zou, Mantas Mazeika, Dawn Song, and Jacob Steinhardt. Measuring massive multitask language understanding. *arXiv preprint arXiv:2009.03300*, 2020.
- [14] Dan Hendrycks, Collin Burns, Saurav Kadavath, Akul Arora, Steven Basart, Eric Tang, Dawn Song, and Jacob Steinhardt. Measuring mathematical problem solving with the math dataset. *arXiv preprint arXiv:2103.03874*, 2021.
- [15] Jordan Hoffmann, Sebastian Borgeaud, Arthur Mensch, Elena Buchatskaya, Trevor Cai, Eliza Rutherford, Diego de Las Casas, Lisa Anne Hendricks, Johannes Welbl, Aidan Clark, et al. Training compute-optimal large language models (2022). *arXiv preprint arXiv:2203.15556*, 2022.
- [16] Haiyang Huang, Newsha Ardalani, Anna Sun, Liu Ke, Hsien-Hsin S Lee, Shruti Bhosale, Carole-Jean Wu, and Benjamin Lee. Toward efficient inference for mixture of experts. *Advances in Neural Information Processing Systems*, 37:84033–84059, 2024.

---

- [17] Hongzhi Huang, Defa Zhu, Banggu Wu, Yutao Zeng, Ya Wang, Qiyang Min, and Xun Zhou. Over-tokenized transformer: Vocabulary is generally worth scaling. *arXiv preprint arXiv:2501.16975*, 2025.
- [18] Yuzhen Huang, Yuzhuo Bai, Zhihao Zhu, Junlei Zhang, Jinghan Zhang, Tangjun Su, Junteng Liu, Chuancheng Lv, Yikai Zhang, Yao Fu, et al. C-eval: A multi-level multi-discipline chinese evaluation suite for foundation models. *Advances in Neural Information Processing Systems*, 36:62991–63010, 2023.
- [19] Zihao Huang, Qiyang Min, Hongzhi Huang, Defa Zhu, Yutao Zeng, Ran Guo, and Xun Zhou. Ultra-sparse memory network. *arXiv preprint arXiv:2411.12364*, 2024.
- [20] Naman Jain, King Han, Alex Gu, Wen-Ding Li, Fanjia Yan, Tianjun Zhang, Sida Wang, Armando Solar-Lezama, Koushik Sen, and Ion Stoica. Livecodebench: Holistic and contamination free evaluation of large language models for code. *arXiv preprint arXiv:2403.07974*, 2024.
- [21] Shibo Jie, Yehui Tang, Kai Han, Yitong Li, Duyu Tang, Zhi-Hong Deng, and Yunhe Wang. Mixture of lookup experts. *arXiv preprint arXiv:2503.15798*, 2025.
- [22] Mandar Joshi, Eunsol Choi, Daniel S Weld, and Luke Zettlemoyer. Triviaqa: A large scale distantly supervised challenge dataset for reading comprehension. *arXiv preprint arXiv:1705.03551*, 2017.
- [23] Jared Kaplan, Sam McCandlish, Tom Henighan, Tom B Brown, Benjamin Chess, Rewon Child, Scott Gray, Alec Radford, Jeffrey Wu, and Dario Amodei. Scaling laws for neural language models. *arXiv preprint arXiv:2001.08361*, 2020.
- [24] Konwoo Kim, Suhas Kotha, Percy Liang, and Tatsunori Hashimoto. Pre-training under infinite compute. *arXiv preprint arXiv:2509.14786*, 2025.
- [25] Yechan Kim, Hwijoon Lim, and Dongsu Han. Scaling beyond the gpu memory limit for large mixture-of-experts model training. In *Forty-first International Conference on Machine Learning*, 2024.
- [26] Diederik P Kingma. Adam: A method for stochastic optimization. *arXiv preprint arXiv:1412.6980*, 2014.
- [27] Jakub Krajewski, Jan Ludziejewski, Kamil Adamczewski, Maciej Pióro, Michał Krutul, Szymon Antoniak, Kamil Ciebiera, Krystian Król, Tomasz Odrzygóźdż, Piotr Sankowski, et al. Scaling laws for fine-grained mixture of experts. *arXiv preprint arXiv:2402.07871*, 2024.
- [28] Jakub Krajewski, Marcin Chochowski, and Daniel Korzekwa. Scaling fine-grained moe beyond 50b parameters: Empirical evaluation and practical insights. *arXiv preprint arXiv:2506.02890*, 2025.
- [29] Guillaume Lample, Alexandre Sablayrolles, Marc’Aurelio Ranzato, Ludovic Denoyer, and Hervé Jégou. Large memory layers with product keys. *Advances in Neural Information Processing Systems*, 32, 2019.
- [30] Haonan Li, Yixuan Zhang, Fajri Koto, Yifei Yang, Hai Zhao, Yeyun Gong, Nan Duan, and Timothy Baldwin. Cmmlu: Measuring massive multitask language understanding in chinese. In *Findings of the Association for Computational Linguistics: ACL 2024*, pp. 11260–11285, 2024.
- [31] Aixin Liu, Bei Feng, Bin Wang, Bingxuan Wang, Bo Liu, Chenggang Zhao, Chengqi Deng, Chong Ruan, Damai Dai, Daya Guo, et al. Deepseek-v2: A strong, economical, and efficient mixture-of-experts language model. *arXiv preprint arXiv:2405.04434*, 2024.
- [32] Aixin Liu, Bei Feng, Bing Xue, Bingxuan Wang, Bochao Wu, Chengda Lu, Chenggang Zhao, Chengqi Deng, Chenyu Zhang, Chong Ruan, et al. Deepseek-v3 technical report. *arXiv preprint arXiv:2412.19437*, 2024.

---

[33] Alisa Liu, Jonathan Hayase, Valentin Hofmann, Sewoong Oh, Noah A Smith, and Yejin Choi. Superbpe: Space travel for language models. *arXiv preprint arXiv:2503.13423*, 2025.

[34] Ilya Loshchilov, Cheng-Ping Hsieh, Simeng Sun, and Boris Ginsburg. ngpt: Normalized transformer with representation learning on the hypersphere. *arXiv preprint arXiv:2410.01131*, 2024.

[35] Anton Lozhkov, Loubna Ben Allal, Leandro von Werra, and Thomas Wolf. Fineweb-edu: the finest collection of educational content, 2024. URL <https://huggingface.co/datasets/HuggingFaceFW/fineweb-edu>.

[36] Huy Nguyen, Nhat Ho, and Alessandro Rinaldo. Sigmoid gating is more sample efficient than softmax gating in mixture of experts. *Advances in Neural Information Processing Systems*, 37: 118357–118388, 2024.

[37] Artidoro Pagnoni, Ramakanth Pasunuru, Pedro Rodriguez, John Nguyen, Benjamin Muller, Margaret Li, Chunting Zhou, Lili Yu, Jason E Weston, Luke Zettlemoyer, et al. Byte latent transformer: Patches scale better than tokens. In *Proceedings of the 63rd Annual Meeting of the Association for Computational Linguistics (Volume 1: Long Papers)*, pp. 9238–9258, 2025.

[38] Tim Pearce and Jinyeop Song. Reconciling kaplan and chinchilla scaling laws. *Transactions on Machine Learning Research*, 2024.

[39] Alec Radford, Jeffrey Wu, Rewon Child, David Luan, Dario Amodei, Ilya Sutskever, et al. Language models are unsupervised multitask learners. *OpenAI blog*, 1(8):9, 2019.

[40] David Rein, Betty Li Hou, Asa Cooper Stickland, Jackson Petty, Richard Yuanzhe Pang, Julien Dirani, Julian Michael, and Samuel R Bowman. Gpqa: A graduate-level google-proof q&a benchmark. In *First Conference on Language Modeling*, 2024.

[41] Maarten Sap, Hannah Rashkin, Derek Chen, Ronan LeBras, and Yejin Choi. Socialqa: Commonsense reasoning about social interactions. *arXiv preprint arXiv:1904.09728*, 2019.

[42] Nikhil Sardana, Jacob Portes, Sasha Doubov, and Jonathan Frankle. Beyond chinchilla-optimal: Accounting for inference in language model scaling laws. *arXiv preprint arXiv:2401.00448*, 2023.

[43] Noam Shazeer, Azalia Mirhoseini, Krzysztof Maziarz, Andy Davis, Quoc Le, Geoffrey Hinton, and Jeff Dean. Outrageously large neural networks: The sparsely-gated mixture-of-experts layer. *arXiv preprint arXiv:1701.06538*, 2017.

[44] Mohammad Shoeybi, Mostofa Patwary, Raul Puri, Patrick LeGresley, Jared Casper, and Bryan Catanzaro. Megatron-lm: Training multi-billion parameter language models using model parallelism. *arXiv preprint arXiv:1909.08053*, 2019.

[45] Kai Sun, Dian Yu, Dong Yu, and Claire Cardie. Investigating prior knowledge for challenging chinese machine reading comprehension. *Transactions of the Association for Computational Linguistics*, 8:141–155, 2020.

[46] Mirac Suzgun, Nathan Scales, Nathanael Schärli, Sebastian Gehrman, Yi Tay, Hyung Won Chung, Aakanksha Chowdhery, Quoc V Le, Ed H Chi, Denny Zhou, et al. Challenging big-bench tasks and whether chain-of-thought can solve them. *arXiv preprint arXiv:2210.09261*, 2022.

[47] Sho Takase, Ryokan Ri, Shun Kiyono, and Takuya Kato. Large vocabulary size improves large language models. *arXiv preprint arXiv:2406.16508*, 2024.

[48] Chaofan Tao, Qian Liu, Longxu Dou, Niklas Muennighoff, Zhongwei Wan, Ping Luo, Min Lin, and Ngai Wong. Scaling laws with vocabulary: Larger models deserve larger vocabularies. *Advances in Neural Information Processing Systems*, 37:114147–114179, 2024.

[49] Changxin Tian, Kunlong Chen, Jia Liu, Ziqi Liu, Zhiqiang Zhang, and Jun Zhou. Towards greater leverage: Scaling laws for efficient mixture-of-experts language models. *arXiv preprint arXiv:2507.17702*, 2025.

---

[50] Ashish Vaswani, Noam Shazeer, Niki Parmar, Jakob Uszkoreit, Llion Jones, Aidan N Gomez, Łukasz Kaiser, and Illia Polosukhin. Attention is all you need. *Advances in neural information processing systems*, 30, 2017.

[51] Pablo Villalobos, Anson Ho, Jaime Sevilla, Tamay Besiroglu, Lennart Heim, and Marius Hobbhahn. Position: Will we run out of data? limits of llm scaling based on human-generated data. In *Forty-first International Conference on Machine Learning*, 2024.

[52] Qiang Wang, Bei Li, Tong Xiao, Jingbo Zhu, Changliang Li, Derek F Wong, and Lidia S Chao. Learning deep transformer models for machine translation. *arXiv preprint arXiv:1906.01787*, 2019.

[53] Kaiyue Wen, Zhiyuan Li, Jason Wang, David Hall, Percy Liang, and Tengyu Ma. Understanding warmup-stable-decay learning rates: A river valley loss landscape perspective. *arXiv preprint arXiv:2410.05192*, 2024.

[54] Samuel Williams, Andrew Waterman, and David Patterson. Roofline: an insightful visual performance model for multicore architectures. *Communications of the ACM*, 52(4):65–76, 2009.

[55] An Yang, Anfeng Li, Baosong Yang, Beichen Zhang, Binyuan Hui, Bo Zheng, Bowen Yu, Chang Gao, Chengan Huang, Chenxu Lv, et al. Qwen3 technical report. *arXiv preprint arXiv:2505.09388*, 2025.

[56] An Yang, Anfeng Li, Baosong Yang, Beichen Zhang, Binyuan Hui, Bo Zheng, Bowen Yu, Chang Gao, Chengan Huang, Chenxu Lv, et al. Qwen3 technical report. *arXiv preprint arXiv:2505.09388*, 2025.

[57] Da Yu, Edith Cohen, Badih Ghazi, Yangsibo Huang, Pritish Kamath, Ravi Kumar, Daogao Liu, and Chiyuan Zhang. Scaling embedding layers in language models. *arXiv preprint arXiv:2502.01637*, 2025.

[58] Rowan Zellers, Ari Holtzman, Yonatan Bisk, Ali Farhadi, and Yejin Choi. Hellaswag: Can a machine really finish your sentence? *arXiv preprint arXiv:1905.07830*, 2019.

[59] Lianmin Zheng, Liangsheng Yin, Zhiqiang Xie, Chuyue Livia Sun, Jeff Huang, Cody Hao Yu, Shiyi Cao, Christos Kozyrakis, Ion Stoica, Joseph E Gonzalez, et al. Sqlang: Efficient execution of structured language model programs. *Advances in neural information processing systems*, 37:62557–62583, 2024.

[60] Defa Zhu, Hongzhi Huang, Zihao Huang, Yutao Zeng, Yunyao Mao, Banggu Wu, Qiyang Min, and Xun Zhou. Hyper-connections. *arXiv preprint arXiv:2409.19606*, 2024.

[61] George Kingsley Zipf. *Human behavior and the principle of least effort: An introduction to human ecology*. Ravenio books, 2016.

---

## A DERIVATIONS FOR JTOK-M SCALING LAWS

Here we provide detailed derivations for Eq. 16 and Eq. 17.

**Step 1: JTOK-M as an effective rescaling of the model-size term.** We start from the Kaplan form (Eq. 5). For JTOK-M, we introduce the effective parameter count

$$N_{\text{eff}} = N_c + \gamma(\rho)N_n = N_c(1 + \eta\gamma(\rho)), \quad \eta \triangleq N_n/N_c. \quad (19)$$

Plugging  $N_{\text{eff}}$  into Eq. 5 yields

$$\begin{aligned} \mathcal{L}_{\text{JTOK-M}}(N_c, D; \eta, \rho) &= \left[ \left( \frac{A}{N_{\text{eff}}} \right)^{\frac{\alpha}{\beta}} + \frac{B}{D} \right]^{\beta} \\ &= \left[ \left( \frac{A/(1 + \eta\gamma(\rho))}{N_c} \right)^{\frac{\alpha}{\beta}} + \frac{B}{D} \right]^{\beta}. \end{aligned} \quad (20)$$

Define

$$A_{\text{JTOK-M}} \triangleq \frac{A}{1 + \eta\gamma(\rho)}. \quad (21)$$

Then JTOK-M has the same functional form as the backbone loss, except that the constant in the model-size term is rescaled from  $A$  to  $A_{\text{JTOK-M}}$ .

**Step 2: Compute-optimal frontier and its dependence on  $A$ .** Under the standard training-FLOPs approximation  $C \approx 6N_c D$  (Sec. 3.1.2), we can write  $D = C/(6N_c)$  and view the loss as a function of  $N_c$  at fixed  $C$ :

$$\mathcal{L}(N_c; C) = \left[ \left( \frac{A}{N_c} \right)^{\frac{\alpha}{\beta}} + \frac{6BN_c}{C} \right]^{\beta}. \quad (22)$$

Minimizing the bracketed term over  $N_c$  gives the compute-optimal frontier  $\mathcal{L}^*(C)$ . A standard calculation for this two-term trade-off (capacity term decays with  $N_c$  while data term grows with  $N_c$  under fixed  $C$ ) yields the well-known dependence

$$\mathcal{L}^*(C) \propto A^{\frac{\alpha\beta}{\alpha+\beta}} C^{-\frac{\alpha\beta}{\alpha+\beta}}, \quad (23)$$

i.e., at compute-optimality the frontier is a power law in  $C$ , and its *intercept* scales as  $A^{\frac{\alpha\beta}{\alpha+\beta}}$ .

Since JTOK-M only changes  $A \mapsto A_{\text{JTOK-M}}$  while keeping the same  $C$ -dependence, we immediately obtain the multiplicative shift:

$$\begin{aligned} \mathcal{L}_{\text{JTOK-M}}^*(C; \eta, \rho) &= \left( \frac{A_{\text{JTOK-M}}}{A} \right)^{\frac{\alpha\beta}{\alpha+\beta}} \mathcal{L}^*(C) \\ &= (1 + \eta\gamma(\rho))^{-\frac{\alpha\beta}{\alpha+\beta}} \cdot \mathcal{L}^*(C), \end{aligned} \quad (24)$$

which is Eq. (16).

**Step 3: Isoperformance compute saving.** Eq. (16) implies that, in the compute-optimal regime, JTOK-M improves the frontier by a *constant* multiplicative factor independent of  $C$ . Let  $k \triangleq \frac{\alpha\beta}{\alpha+\beta}$  and write  $\mathcal{L}^*(C) = \kappa C^{-k}$  for some constant  $\kappa$ . Then Eq. (16) becomes

$$\mathcal{L}_{\text{JTOK-M}}^*(C) = (1 + \eta\gamma(\rho))^{-k} \kappa C^{-k}. \quad (25)$$

For any target loss  $\mathcal{L}^*$ , solving  $\mathcal{L}^* = \kappa(C_{\text{base}}^*)^{-k}$  and  $\mathcal{L}^* = (1 + \eta\gamma(\rho))^{-k} \kappa(C_{\text{JTOK-M}}^*)^{-k}$  gives

$$C_{\text{JTOK-M}}^*(\mathcal{L}^*) = \frac{1}{1 + \eta\gamma(\rho)} C_{\text{base}}^*(\mathcal{L}^*), \quad (26)$$

which is Eq. (17). Notably, the compute saving ratio depends only on JTOK-M hyperparameters through  $(\eta, \rho)$  and  $\gamma(\rho)$ , and is independent of the backbone scale.

---

## B LOAD-BALANCING AUXILIARY LOSS FOR JTOK-M

Similar to MoE architectures that require balanced expert utilization for optimal throughput and learning, JTok-M benefits from uniform routing across its  $n_e$  embedding experts  $\{E_i\}_{i=1}^{n_e}$ . To encourage all embeddings are adequately trained and contribute to model performance, we incorporate an auxiliary load-balancing loss that encourages balanced routing distributions.

**Formulation.** Consider a training batch with  $T$  tokens, where JTok-M maintains  $n_e$  embedding experts and each token routes to top- $K$  embeddings. Let  $G_t \subseteq \{1, \dots, n_e\}$  denote the top- $K$  routing set for token  $t$ , and  $p_t^{(i)} \in [0, 1]$  represent the routing probability of token  $t$  to embedding  $i$ .

We define the following quantities:

- **Aggregate routing probability:**  $P_i = \sum_{t=1}^T p_t^{(i)}$  — the unnormalized sum of routing probabilities for embedding  $i$
- **Actual token count:**  $n_i = \sum_{t=1}^T \mathbf{1}\{i \in G_t\}$  — number of tokens actually routed to embedding  $i$
- **Normalized routing probability:**  $p_i = \frac{P_i}{T}$  — the average routing probability for embedding  $i$
- **Normalized load fraction:**  $f_i = \frac{n_i}{TK}$  — the fraction of total route capacity used by embedding  $i$

The load-balancing auxiliary loss is formulated as:

$$\mathcal{L}_{\text{aux}} = \lambda \cdot n_e \sum_{i=1}^{n_e} p_i f_i = \lambda \cdot \frac{n_e}{T^2 K} \sum_{i=1}^{n_e} P_i n_i \quad (27)$$

where  $\lambda$  is a hyperparameter controlling the strength of the load-balancing constraint.

**Intuition.** The term  $p_i$  captures the expected routing distribution to embedding  $i$ , while  $f_i$  measures its actual utilization. The loss in Equation 27 penalizes the co-occurrence of high routing probability and high actual load, thereby discouraging the concentration of routing on a subset of embeddings. This encourages a more uniform distribution where ideally  $p_i \approx f_i \approx 1/n_e$  for all  $i$ , ensuring that all embeddings receive sufficient training signal and contribute effectively to model capacity.

**Implementation.** In practice, we compute this auxiliary loss per layer and average across all JTok-M layers. The hyperparameter  $\lambda$  is typically set to  $10^{-4}$ , balancing load distribution without overwhelming the primary language modeling objective. This auxiliary loss is added to the main cross-entropy loss during training and is automatically handled by the backward pass without requiring special gradient computation.

## C DETAILED COMPUTE-OPTIMAL SCALING LAWS

In this section, we provide the detailed numerical results and linear fitting parameters for the IsoFLOPs analysis discussed in Sec. 4.2.1. We compare the compute-optimal performance of the vanilla MoE backbone against the JTok-M augmented variant ( $\eta = 50, \rho = 0.25$ ) across five orders of magnitude of compute budgets.

### C.1 COMPUTE-OPTIMAL DATA POINTS

Table 4 lists the compute-optimal test losses ( $\mathcal{L}^*$ ) for both the vanilla MoE backbone and the JTok-M model at five distinct FLOPs budgets ( $C$ ). These values correspond to the minima of the IsoFLOPs curves. The relative improvement is calculated as  $1 - (\mathcal{L}_{\text{JTOK-M}}^* / \mathcal{L}_{\text{Base}}^*)$ .

### C.2 LINEAR FITTING OF EFFICIENT FRONTIERS

To characterize the scaling behavior, we perform a linear regression in the log-log space. Following the standard practice, we use  $\log_{10}$  for the compute budget  $C$  and  $\log_2$  for the loss  $L$  (to align with previous work numerical scales). The relationship is modeled as:

$$\log_2(\mathcal{L}) = \alpha \cdot \log_{10}(C) + \beta \quad (28)$$

Based on the data points in Table 4, we obtain the following linear fits:

Table 4: Compute-optimal test loss comparison between Vanilla MoE and JTok-M across different compute budgets. The data corresponds to the extracted efficient frontiers.

Budget ( $C$ ) (FLOPs)	Vanilla MoE ( $\mathcal{L}_{\text{Base}}^*$ )	JTok-M ( $\mathcal{L}_{\text{JTok-M}}^*$ )
$3 \times 10^{18}$	2.6537	2.5981
$1 \times 10^{19}$	2.4569	2.3999
$3 \times 10^{19}$	2.3065	2.2521
$1 \times 10^{20}$	2.1422	2.0969
$3 \times 10^{20}$	2.0176	1.9726

#### Vanilla MoE (Backbone)

$$\log_2(\mathcal{L}) = -0.2016 \cdot \log_{10}(C) + 5.1334, \quad R^2 = 0.9994 \quad (29)$$

#### JTok-M

$$\log_2(\mathcal{L}) = -0.2009 \cdot \log_{10}(C) + 5.0881, \quad R^2 = 0.9991 \quad (30)$$

### C.3 DERIVATION OF COMPUTE SAVING RATIO

In this subsection, we provide the mathematical derivation for the 35% compute saving claim based on the fitted efficient frontiers.

**Formulation** Let the scaling laws for the baseline and JTok-M models be expressed in the log-log space as:

$$\log_2(\mathcal{L}_{\text{base}}) = \alpha \cdot \log_{10}(C) + \beta_{\text{base}} \quad (31)$$

$$\log_2(\mathcal{L}_{\text{JTok-M}}) = \alpha \cdot \log_{10}(C) + \beta_{\text{JTok-M}} \quad (32)$$

where  $\alpha$  represents the scaling slope (empirically  $\approx -0.2016$ ) and  $\beta$  represents the intercept. We assume the slopes are identical based on the empirical fits shown in Fig. 6a.

**Compute Ratio for Iso-Loss** To estimate the compute saving, we determine the ratio of compute budgets ( $C_{\text{JTok-M}}$  vs.  $C_{\text{base}}$ ) required to achieve the same target validation loss  $\mathcal{L}^*$ . Setting  $\mathcal{L}_{\text{base}}(C_{\text{base}}) = \mathcal{L}_{\text{JTok-M}}(C_{\text{JTok-M}}) = \mathcal{L}^*$ :

$$\alpha \cdot \log_{10}(C_{\text{base}}) + \beta_{\text{base}} = \alpha \cdot \log_{10}(C_{\text{JTok-M}}) + \beta_{\text{JTok-M}} \quad (33)$$

Rearranging the terms to solve for the compute ratio:

$$\alpha(\log_{10}(C_{\text{JTok-M}}) - \log_{10}(C_{\text{base}})) = \beta_{\text{base}} - \beta_{\text{JTok-M}} \quad (34)$$

$$\log_{10}\left(\frac{C_{\text{JTok-M}}}{C_{\text{base}}}\right) = \frac{\beta_{\text{base}} - \beta_{\text{JTok-M}}}{\alpha} = \frac{\Delta\beta}{\alpha} \quad (35)$$

Thus, the compute ratio is given by:

$$\text{Ratio} = \frac{C_{\text{JTok-M}}}{C_{\text{base}}} = 10^{\frac{\Delta\beta}{\alpha}} \quad (36)$$

**Calculation** Using the fitted parameters from our experiments:

- Slope  $\alpha \approx -0.2016$
- Intercept difference  $\Delta\beta = \beta_{\text{base}} - \beta_{\text{JTok-M}} \approx 0.038$

Substituting these values:

$$\text{Ratio} = 10^{\frac{0.038}{-0.2016}} \approx 10^{-0.1885} \approx 0.648 \quad (37)$$

Finally, the compute saving is:

$$\text{Saving} = 1 - \text{Ratio} = 1 - 0.648 \approx 35.2\% \quad (38)$$

This confirms that JTok-M reduces the compute budget required to reach a target loss by approximately 35%.

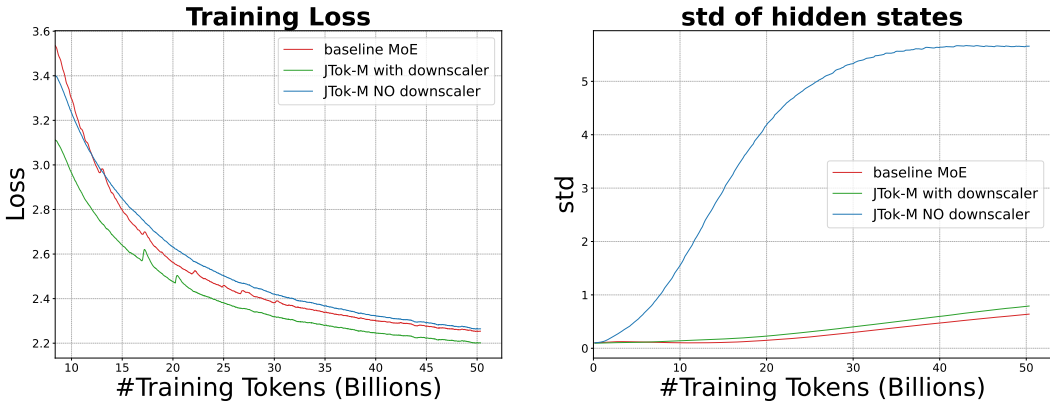


Figure 7: Ablation of the scaling factor  $\frac{1}{\sqrt{2N_l}}$  in JTOK-M. Left: training loss. Right: averaged std of hidden states over layers and tokens.

## D ABLATION STUDIES

### D.1 SCALING FACTOR $\frac{1}{\sqrt{2N_l}}$ IN JTOK-M

To stabilize the variance of hidden states when injecting JTOK-M residuals, we scale the modulation update in each layer with a factor  $\frac{1}{\sqrt{2N_l}}$  (Eq. 12).

We perform an ablation on the 3.2B–A0.5B MoE backbone comparing (i) the baseline(backbone MoE), (ii) JTOK-M *with* the scaling factor (our default), and (iii) JTOK-M *without* the scaling factor. All models are trained under identical data and optimization settings.

Fig. 7 (left) reports the training loss, while Fig. 7 (right) shows the standard deviation of hidden states averaged over all layers and tokens. Without the scaling factor, the activation std grows rapidly to above 5.5 within the first 50B training tokens and the model underperforms the baseline MoE in terms of loss. In contrast, JTOK-M with the proposed  $\frac{1}{\sqrt{2N_l}}$  factor keeps variance of hidden states close to baseline in a well-behaved range and consistently achieves lower training loss than the baseline. These results confirm that the scaling factor is crucial to prevent variance explosion and to ensure that JTOK-M’s modulation effectively improves optimization.

### D.2 NORM IN JTOK/JTOK-M

JTok augments each layer with a token-indexed modulation vector retrieved from an embedding table, as described in Section 3.2.

**Why normalizing the modulation vector matters.** At a high level, JTOK aims to provide *token-specific* and dimension-wise modulation. In this mechanism, the direction of  $\mathbf{E}^\ell[x]$  encodes how the residual update should be modulated across hidden dimensions, whereas its magnitude primarily controls the overall strength of that modulation. Applying  $\text{Norm}_\varepsilon(\cdot)$  explicitly removes the magnitude degree of freedom and places the modulation vector on a hypersphere.

This has two practical benefits.

**1. Better-conditioned optimization: learning direction without chasing scale.** Without normalization, the gate depends on the raw embedding magnitude, so training needs to jointly tune both direction and norm of  $\mathbf{E}^\ell[x]$  to reach an effective modulation regime. In long-horizon training with Adam-style optimizers, the effective step magnitude in parameter space is typically bounded by the scheduled learning rate (up to the factor  $m/\sqrt{v}$ ), and in common regimes one often has  $m/\sqrt{v} \approx \mathcal{O}(1)$  [26; 34]. Therefore, as  $\mathbf{E}^\ell[x]$  is usually initialized at a small scale [31], its norm tends to remain  $\mathcal{O}(1)$  for a long time unless gradients consistently push in the radial direction. This makes it difficult for the model to quickly reach the “right” modulation strength through embedding norms alone. Normalization resolves this by decoupling direction learning from scale: the token embedding focuses on learning a direction on the hypersphere, while the learnable per-dimension

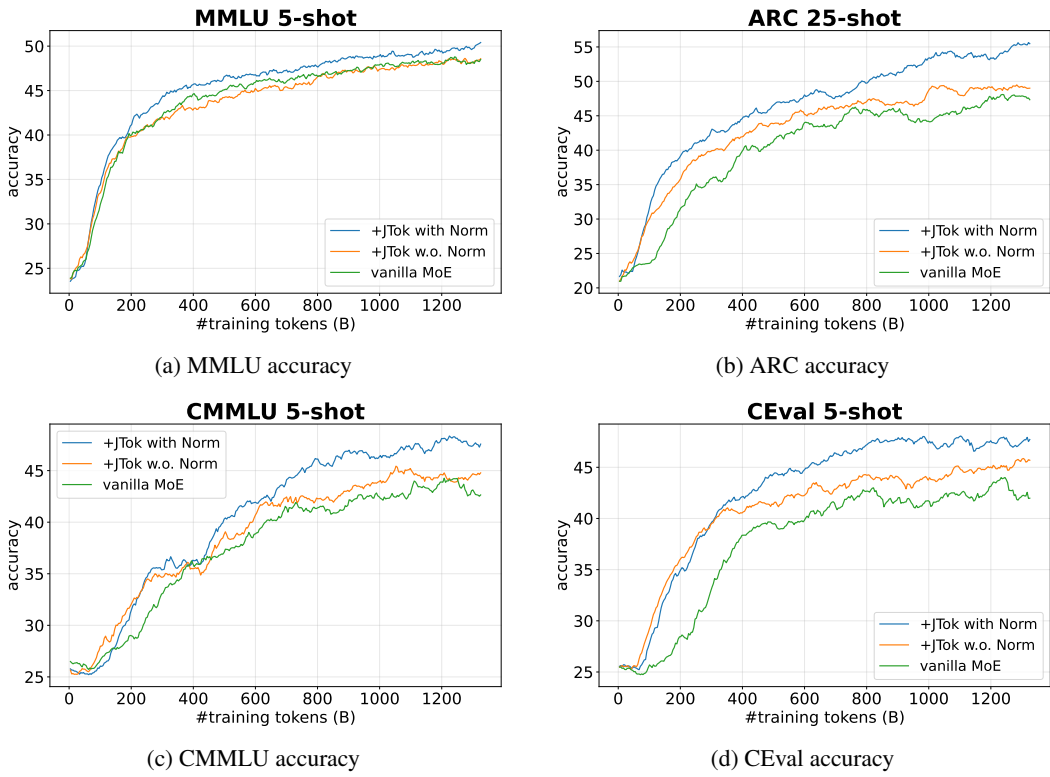


Figure 8: **Normalization ablation for JTOK.** Downstream accuracy trajectories on MMLU, ARC, CMMLU, and CEval during long-horizon pretraining ( $\sim 1.3T$  tokens) on the 3.2B-A0.5B MoE backbone, comparing backbone-only, JTOK with norm, and JTOK without norm. Applying norm consistently accelerates convergence and improves the final accuracy across all benchmarks, indicating that hypersphere-normalized modulation yields more stable optimization and a higher performance ceiling.

scaler  $s^\ell$  controls the overall modulation strength. Although normalization fixes one scalar degree of freedom, it retains essentially all expressive power in high dimensions. Noting that a  $d$ -dimensional vector on the hypersphere still has  $d - 1$  degrees of freedom.

**2. Stable and comparable modulation across tokens.** Token-indexed tables can have highly non-uniform access frequencies, which leads to heterogeneous gradient statistics across token embeddings. Without normalization, different tokens can drift to different norms, making the gate distribution highly inconsistent and potentially harming stability (e.g., some tokens barely modulate while others over-modulate). By constraining all retrieved vectors to a comparable norm, it produces a more predictable gate scale across tokens and layers, making the plugin behave like a controlled residual modulation.

**Experimental setup.** We conduct an ablation on the 3.2B-A0.5B MoE backbone, comparing three variants: (i) backbone-only, (ii) JTOK w/ norm using  $\text{Norm}_\varepsilon$  as above, and (iii) JTOK w.o. norm where the retrieved vector is used directly without normalization. All runs use the same architecture and training recipe; to better expose optimization differences, we intentionally *overtrain* to  $\sim 1.3T$  tokens and periodically evaluate downstream accuracy throughout training. We report MMLU, ARC, CMMLU, and CEval trajectories in Fig. 8.

**Results and discussion.** Fig. 8 shows that normalization substantially improves both optimization speed and final performance. Across all four benchmarks, JTOK w/ norm rises faster in the early-to-mid training regime and consistently maintains a higher accuracy curve than JTOK w.o. norm. Moreover, the gap persists (or even widens) even under long training, indicating that normalization is not merely a transient stabilization trick but also enables JTOK to realize a higher effective capacity ceiling.

Table 5: Hyper-parameters for dense model pretraining.

	Parameters	small	medium	large	XL
Optimizer	lr-schedule	cosine	cosine	cosine	WSD [53]
	max, min lr	(1e-3, 1e-4)	(8e-4, 8e-5)	(6e-4, 6e-5)	(6e-4, 0)
	warmup-ratio			0.05	
	decay-ratio	0.95	0.95	0.95	0.00
	optimizer			AdamW [26]	
	weight-decay			0.1	
JTok	grad.clip			1.0	
	#extra params.	464M	1.2B	2.3B	6.5B

Table 6: Hyper-parameters for MoE model pretraining.

	Parameters	1.5B-A250M	3.2B-A0.5B	17B-A2B
Optimizer	lr-schedule		WSD	
	lr		4.2e-4	
	warmup-ratio		0.05	
	decay-ratio		0.00	
	optimizer		AdamW	
	weight-decay		0.1	
Backbone	grad.clip		1.0	
	hidden dim.	512	768	2048
	#dense layers	1	1	1
	#moe layer	11	17	27
	#q heads	8	16	16
	#kv heads	4	4	8
	context-length	8192	8192	8192
	#routed experts	144	144	64
	# shared experts		1	
	topK route	8	8	6
Data	dense FFN size		10944	
	MoE FFN size	512	512	1408
	#tokens(B)	300	500	570
JTok	#extra params.	934M	2.1B	-
JTOK-M	$n_e$		5	
	K		2	
	#extra params.	4.7B	10.5B	43.6B

## E DETAILED TRAINING AND MODEL HYPERPARAMETERS

Table 5 provides the pretraining hyperparameters for dense models, covering four model sizes (small, medium, large, and XL) and their JTOK variants. Table 6 shows the pretraining hyperparameters for MoE models, specifically two configurations (1.5B-A250M, 3.2B-A0.5B and 17B-A2B) together with their JTOK and JTOK-M variants.